Article

# Phase Behavior and Superprotonic Conductivity in the System $(1-x)CsH_2PO_4 - xH_3PO_4$: Discovery of Off-Stoichiometric $\alpha$-$[Cs_{1-x}H_x]H_2PO_4$

Louis S. Wang, Sawankumar V. Patel, Erica Truong, Yan-Yan Hu, and Sossina M. Haile*

Read Online

ACCESS | Metrics & More | Article Recommendations | SI Supporting Information

**ABSTRACT:** $CsH_2PO_4$ has garnered interest as a proton-conducting electrolyte due to its exceptional conductivity at intermediate temperatures (228−300 °C) at which it adopts a cubic structure with a high degree of disorder. Here, through a study of mixtures of $CsH_2PO_4$ (CDP) and $CsH_5(PO_4)_2$, the cubic phase was discovered to form solid solutions of composition $[Cs_{1-x}H_x]H_2PO_4$, with $x$ extending to at least 2/9. A phase diagram of the composition space $(1-x)CsH_2PO_4 - xH_3PO_4$, $0 \leq x \leq 2/9$ was developed through thermal analysis, high-temperature in situ X-ray diffraction experiments, and variable-temperature NMR spectroscopy. At temperatures above about 90 °C, monoclinic, stoichiometric CDP exists in equilibrium with $Cs_7(H_4PO_4)$-$(H_2PO_4)_8$. These two phases displayed eutectoid behavior, with a eutectoid reaction temperature and composition of 155 °C and $x = 0.18$, respectively, to form cubic $[Cs_{1-x}H_x]H_2PO_4$. The structural studies revealed, rather remarkably, that the cubic phase accommodates vacancies on the cation site that are charge-balanced by excess protons, where the latter are chemically associated with phosphate groups. The conductivities of cubic phases of various compositions, measured by impedance spectroscopy, are comparable to that of CDP. The excellent proton conductivities of off-stoichiometric, cubic $[Cs_{1-x}H_x]H_2PO_4$ at temperatures well below the superprotonic transition of stoichiometric CDP present the opportunity to extend the low-temperature operating limit of CDP-based devices. More generally, the off-stoichiometric phase behavior demonstrated here introduces a new approach for the modification of superprotonic solid acid compounds.
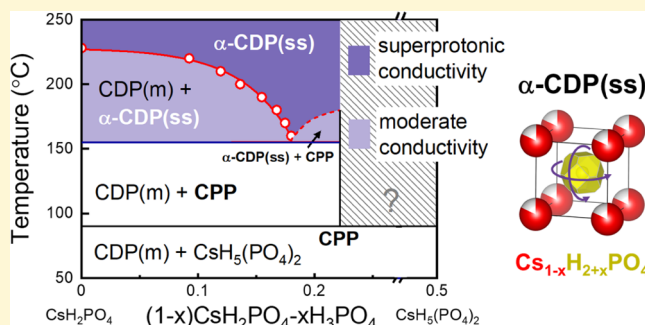
## 1. INTRODUCTION

Solid acid materials with dynamically disordered hydrogen-bond networks[1,2] have garnered interest as electrolytes due to their exceptional proton conductivities at intermediate temperatures (in the approximate range of 100−300 °C). These superprotonic compounds are composed of metal cations, typically alkali metals (Cs, Rb, K), and acidic oxyanions, typically protonated $PO_4$, $SeO_4$, and $SO_4$. At slightly elevated temperatures, the materials adopt disordered crystalline arrangements characterized by rapid oxyanion reorientation and highly mobile disordered protons. These superprotonic phases can exhibit conductivities that exceed $10^{-2}$ S cm$^{-1}$.[3,4]

Among the known superprotonic solid acid materials, only $CsH_2PO_4$ (CDP) has been employed to any significant extent in technologically relevant device demonstration and deployment. This is primarily because only the phosphate anion displays the requisite chemical stability in both oxidizing and reducing environments for device operability.[4−6] Solid acids incorporating $SO_4$ and $SeO_4$ groups generally react with hydrogen to generate $H_2S$ and $H_2Se$ byproducts, respectively.[7] The superprotonic transition in CDP occurs at 228 °C and results in a transformation from a low-temperature monoclinic

phase to a superprotonic cubic phase with a CsCl-like structure with orientationally disordered $H_2PO_4^-$ anions.[4,8,9] At 250 °C, the proton conductivity is $2.5 \times 10^{-2}$ S cm$^{-1}$.[4,8] While the transport properties and redox stability of CDP are well suited for a range of electrochemical applications, there has been some interest in extending the range of superprotonic conductivity to below 228 °C and/or increasing the conductivity of the low-temperature phase so as to minimize possible challenges with the 3 orders of magnitude increase in conductivity at the superprotonic phase transition. Approaches to achieving these goals include preparation of composites,[10−15] homogeneous doping[16,17] (via substitutional elements in the CDP structure), and heterogeneous doping[18−20] (via introduction of secondary components, which can be considered a form of composite preparation).
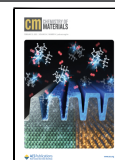
Of the strategies employed to improve the overall properties of CDP, recent work of Ponomareva and co-workers is intriguing for its use of additives such as $CsH_5(PO_4)_2$ and $H_3PO_4$[20], and $Cs_2HPO_4 \cdot H_2O$ and $Cs_3(H_{1.5}PO_4)_2$[18] to CDP, described by those authors to be heterogeneous dopants. In all cases, the additives increased the conductivity at temperatures below the superprotonic transition with minimal impact on the high-temperature conductivity and, in some cases, also improved stability against dehydration. In parallel with this work, we recently showed the existence of the new compound $Cs_7(H_4PO_4)(H_2PO_4)_8$ or CPP, which forms at 90 °C through the stoichiometric reaction of CDP and $CsH_5(PO_4)_2$.[21] This compound is structurally similar to CDP with rotationally disordered phosphate anions arranged in an approximately simple cubic arrangement. It differs from CDP in that one in eight cations is the unusual polycation group $H_4PO_4^+$, and the ordered arrangement of these species generates a cell that has a $4 \times 4 \times 4$ superstructure relative to conventional superprotonic CDP. The compound exhibits a moderate conductivity of $5.8 \times 10^{-4}$ S cm$^{-1}$ at 140 °C and was found to be thermally stable under nominally dry Ar to ≈150 °C.

The existence of CPP indicates that the phase behavior of mixtures of CDP and $CsH_5(PO_4)_2$ must be more complex than suggested by the concept of heterogeneous doping. Accordingly, we undertake here a systematic study of the $(1-x)CsH_2PO_4 - xH_3PO_4$ system from $x = 0$ (CDP) to $x = 2/9$ (CPP). We find at temperatures above 90 °C a two-phase region composed of stoichiometric monoclinic CDP and stoichiometric CPP. At further elevated temperatures, we observe solution behavior and find that cubic CDP, previously considered to be a compound of fixed stoichiometry in the $Cs_3PO_4 - H_3PO_4$ phase space, in fact, exists over a wide composition range. We show that the structural chemistry in the solid solution region is described macroscopically according to $[Cs_{1-x}H_x]H_2PO_4$ and explore the impact of Cs deficiency on the proton transport properties. The insights presented here open up a new approach to modifying the physical and chemical properties of superprotonic solid acids.

## 2. METHODS

Crystals of CDP and $CsH_5(PO_4)_2$ were independently grown from stoichiometric aqueous solutions of $CsCO_3$ and phosphoric acid by evaporation. Samples of various compositions were created from these crystals, which were ground together and homogenized in a mortar and pestle. Dense compacts of each sample were obtained by uniaxial pressing, and the samples were subsequently annealed at elevated temperature for several (1−3) days with the introduction of humidity as required to prevent dehydration. In the case of compositions $x = 2/9$ and 0.18, this step was carried out at 130 °C under dry $N_2$, whereas for compositions $0 < x < 0.18$, the temperature was 230 °C and the atmosphere humidified $N_2$ (steam partial pressure, $pH_2O = 0.4$ atm). X-ray diffraction of the annealed samples, collected after exposure to ambient temperature for several (3−14) days, revealed the original precursor phases in the anticipated relative quantities (as shown, for example, for the $x = 0.07$ material, Figure S1), despite the sluggishness of the reverse transition returning the high-temperature phase(s) to a mixture of CDP(m) and $CsH_5(PO_4)_2$. Here, the combination of long time at ambient temperature and additional grinding for XRD measurement is presumed to have accelerated the reverse reaction. The annealing step was found to improve kinetics for the various phase transitions during heating, likely due to enhanced contact between particles of different phases, and thus all measurements reported here are from annealed, reground samples.

**2.1. Thermal Analysis.** The thermodynamics of various processes (phase transitions, phase formation reactions, dehydration reactions) were measured by simultaneous thermogravimetric analysis (TGA) and differential scanning calorimetry (DSC) using a Netzsch STA F3 equipped with a water vapor generator. Just prior to measurement, annealed compacts were ground and powder samples (∼60 mg) were lightly pressed into platinum pans. Measurements were conducted with Ar-protective and carrier gas streams, and a 1 °C/min heating rate was used in all ramp steps. Steam was produced by the water vapor generator and introduced during 2 h isothermal holds at 130 °C to create highly humidified atmospheres ($pH_2O = 0.4−0.6$ atm). The humidified atmosphere was maintained at all temperatures above 130 °C.

**2.2. X-ray Diffraction.** High-temperature X-ray diffraction (HTXRD) measurements were conducted on a Rigaku Ultima diffractometer with an in-house constructed stage that allowed for active humidification of the sample atmosphere. A $N_2$ gas stream was passed through a temperature-controlled bubbler to create various levels of humidification ($pH_2O = 0.4−0.7$ atm) prior to entering the sample chamber. Humidified gas flow was supplied only at sample temperatures above 130 °C. Samples (again, ground powders from annealed compacts) were heated at a ramp rate of 1 °C/min and held at each temperature for 20 min before measurement. Diffraction patterns were collected with a 5° 2$\theta$/min scan rate and a 0.3° step size. Rietveld refinement against the diffraction patterns to obtain lattice parameters and phase fractions was performed using the software GSAS-II and the established structures of the relevant phases (monoclinic CDP, monoclinic $CsH_5(PO_4)_2$, cubic CDP, and cubic CPP).

**2.3. NMR.** Further structural characterization was achieved through high-temperature solid-state $^1$H and $^{31}$P magic angle spinning (MAS) nuclear magnetic resonance (NMR) spectroscopy. All NMR spectra were collected on a Bruker spectrometer at a Larmor frequency of 500 MHz for $^1$H and 202 MHz for $^{31}$P, using a laser MAS probe at a spin rate of 4 kHz. Powder samples were packed into a 4 mm insert, which was loaded into a 7 mm rotor and placed into the probe. Variable-temperature $^1$H and $^{31}$P NMR spectra were collected between room temperature and 200 °C. For $^1$H NMR measurements below 160 °C, a spin-echo pulse sequence was used with a $\pi/2$-pulse length of 4.40 $\mu$s and a recycle delay of 500 s. At 160 °C, the recycle delays were optimized and a 10 s delay was used for all subsequent measurements above 160 °C. For $^{31}$P NMR measurements, a single $\pi/2$-pulse of 5.00 $\mu$s was applied with a recycle delay of 1000 s for low temperatures, which was then changed to 30 s for measurements at 160 °C and above. An inversion recovery pulse sequence was used to determine the $T_1$ relaxation times for $^1$H and $^{31}$P at temperatures between 160 and 200 °C. In all measurements, 10 min of temperature equilibration was allowed at each step prior to data acquisition. The $^{31}$P NMR shifts were calibrated using $(NH_4)_2HPO_4$ with a $^{31}$P resonance at 1.34 ppm. The $^1$H NMR shifts were calibrated using adamantane with a $^1$H resonance at 1.83 ppm. Sample heating was achieved using a diode laser, and temperature values were calibrated using $^{79}$Br NMR of dry KBr.

**2.4. Impedance Spectroscopy.** Dense compacts for conductivity measurements, roughly 1 mm thick, were prepared by pressing powder samples at 280 MPa for 5 min and then at 390 MPa for 5 min, achieving >92% theoretical density. Silver electrodes, ∼100 nm in thickness, were sputtered on each side. AC impedance spectra were collected at temperatures from 60 to 250 °C in a flowing $N_2$ atmosphere (40 sccm). At temperatures of 130 °C and above, the $N_2$ gas was humidified to either 0.69 atm of steam (for samples $x = 0.18, 0.15,$ and 0.07) or 0.47 atm of steam (for samples $x = 0.05$ and 0.02). Humidification was achieved by passing the gas stream through a bubbler maintained at either 90 or 80 °C, respectively. The conductivity of stoichiometric $CsH_2PO_4$ was also measured as a reference. The samples were held at each measurement temperature for 30 min prior to recording impedance, with a heating rate of 2 °C/min applied between steps. Data were collected using an Agilent 4284A LCR analyzer over the frequency range of 20−10$^5$ Hz with a 20 mV amplitude. Impedance data were analyzed using the commercial software package ZView.

## 3. RESULTS AND DISCUSSION

The phase diagram of the $(1-x)CsH_2PO_4 - xH_3PO_4$ system in the $CsH_2PO_4$-rich region, as deduced from the thermal, XRD, and NMR studies described in detail below, is shown in Figure 1. The compounds CDP, CPP, and $CsH_5(PO_4)_2$ all



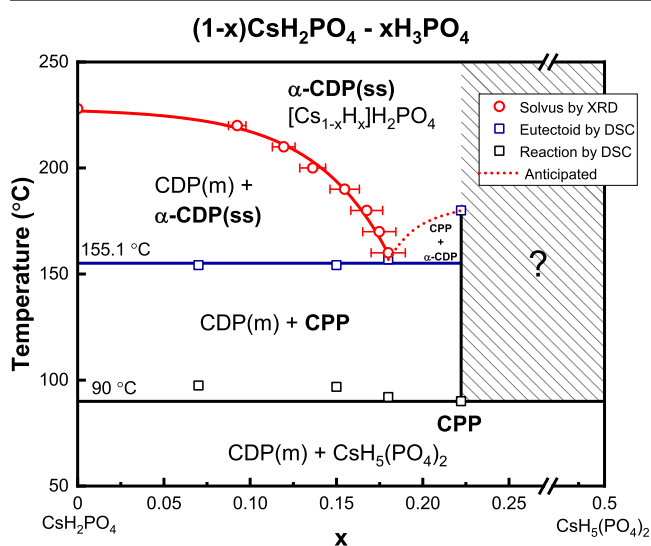**Figure 1.** Phase diagram of the $(1-x)CsH_2PO_4 - xH_3PO_4$ system in the Cs-rich region.

occur in this system. A remarkable finding here is that the cubic superprotonic phase of CDP can accommodate a high level of Cs deficiency by forming vacancies on the cation site that are charge-balanced by excess protons. The resulting composition is $[Cs_{1-x}H_x]H_2PO_4$ and, recognizing the compositional variability, the cubic phase is hereafter designated $\alpha$-CDP(ss), where ss = solid solution. This compound exhibits eutectoid behavior with a eutectoid composition and temperature of $x = 0.18$ and $T = 155$ °C, respectively.

**3.2. Direct Characterization of Phase Behavior.** The phase transformation behavior of three compositions in the $(1-x)CsH_2PO_4 - xH_3PO_4$ system is summarized in Figures 2−6. The examples selected correspond to (i) CPP, $x = 2/9$ (Figure 2), with selected data taken from our previous work,[21] (ii) the eutectoid composition, $x = 0.18$ (Figures 3−5), and (iii) a representative composition rich in Cs relative to the eutectoid, $x = 0.07$ (Figure 6). The data reported are the simultaneous DSC/TGA profiles (with corresponding dTG profiles in Figure S2) and in situ diffraction patterns for all three compositions, along with variable-temperature NMR spectra for the eutectic composition. Thermal analysis data for an additional composition in the Cs-rich region ($x = 0.15$) are provided in the Supporting Information (Figure S3).

For all samples, the ambient temperature diffraction patterns (example shown in Figure S1) revealed a mixture of monoclinic CDP [hereafter CDP(m)] and $CsH_5(PO_4)_2$ phases. For the material of global composition $x = 2/9$, the mixture of CDP(m) and $CsH_5(PO_4)_2$ reacted at 90 °C to form stoichiometric CPP, a result that is consistent with what we have reported previously.[21] This reaction is revealed by an endothermic event that occurs without mass loss at 90 °C (Figure 2a) and in the diffraction pattern collected at 110 °C (Figure 2b). In highly humidified atmospheres ($pH_2O = 0.6$ atm), further heating produced a second sharp thermal
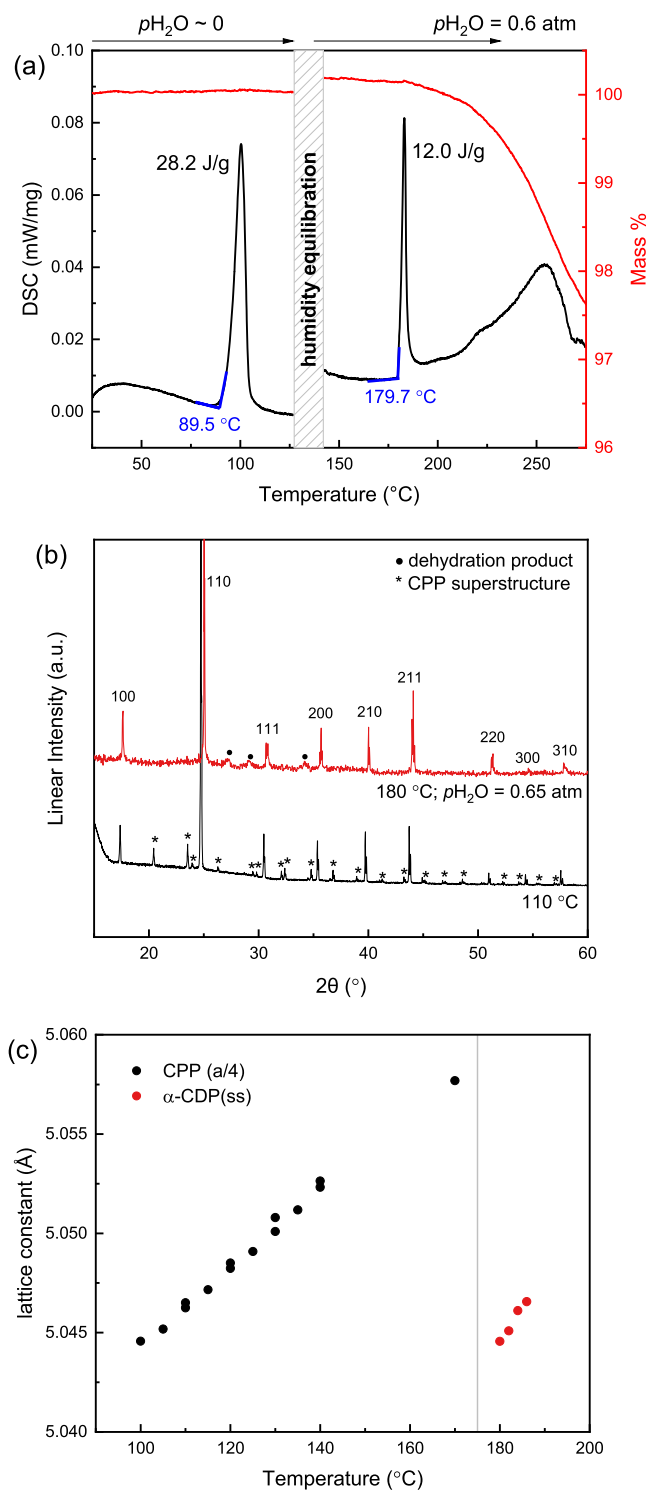


**Figure 2.** Phase transformation behavior of $(1-x)CsH_2PO_4 - xH_3PO_4$ at $x = 2/9$, the composition corresponding to the compound $Cs_7(H_4PO_4)(H_2PO_4)_8$ or CPP: (a) simultaneously measured TGA/DSC profiles at a heating rate of 1 °C/min (data from ref 21 with permission from the American Chemical Society); (b) XRD patterns measured at the temperatures and $pH_2O$ values indicated ($T = 110$ °C, pattern from ref 21 with permission from the American Chemical Society); and (c) lattice constant as a function of temperature (uncertainties in the refined values fall within the span of the datapoint symbols, Figure S4). In (a), $pH_2O = 0.6$ atm (balance Ar) was introduced at 130 °C as part of the heating protocol, and data reflecting system equilibration to the high-humidity condition are

**Figure** 2. continued

omitted. The results reveal the transitions CDP(m) + $CsH_5(PO_4)_2$ → CPP @ 90 °C and CPP → $\alpha$-CDP(ss) @ 180 °C.

anomaly at 180 °C. While mass loss quickly followed this thermal event, the event itself was independent of mass loss. This transition was noted in our previous work; however, we had not fully established its nature.[21] Here, we find the transition to correspond to the complete transformation of CPP to a simple cubic phase, Figure 2b ($T$ = 180 °C). The lattice constant of this new phase, $a$ = 5.0445(7) Å, is substantially smaller than the subcell lattice parameter of CPP, 5.0577(7) Å at 175 °C, indicating a contraction in molar volume at the transition (Figure 2c). Rietveld refinement (Figure S4) showed the 180 °C pattern to be consistent with the structure of cubic superprotonic CDP (CsCl-type, space group $Pm\bar{3}m$), with the exception of a difference in cell parameter. Stoichiometric cubic CDP, which exists only at temperatures of 228 °C and higher, has a cell parameter of 4.970(3)Å at 250 °C,[6] significantly smaller than that of the material encountered here. Recognizing this new material to share the phase space of stoichiometric, $CsH_2PO_4$, it is designated $\alpha$-CDP(ss), where ss = solid solution. Except for the unusual subcell contraction at the transition from CPP to $\alpha$-CDP(ss), the thermal expansion behavior of $\alpha$-CDP(ss) encountered at this composition is rather standard (Figure 2c).

The eutectoid composition sample ($x$ = 0.18) similarly revealed a reaction between CDP(m) and $CsH_5(PO_4)_2$ at 90 °C to form CPP, as indicated by a sharp endothermic peak at this temperature (Figure 3a). In this case, however, the CPP product appeared in equilibrium with excess CDP(m) (Figure 3b, $T$ = 140 °C pattern). This two-phase mixture was stable up to 157 °C, at which temperature CDP(m) and CPP underwent further reaction, as indicated by a second large, binodal, and extended endothermic feature in the DSC profile (Figure 3a). The diffraction pattern collected at 160 °C revealed the reaction to correspond to the complete transformation to a simple cubic phase with lattice constant 5.0277(3) Å and hence the formation of $\alpha$-CDP(ss). As was the case for the $x$ = 2/9 sample, the absence of mass loss upon the formation of $\alpha$-CDP(ss) implies that the composition of the cubic phase is equal to that of the global sample. The overall shape of the DSC signal associated with the eutectoid reaction, a binodal peak followed by a long tail, is somewhat unusual. This behavior, which was not observed for $x$ = 2/9, is tentatively ascribed to the timescale of interdiffusion between CDP(m) and CPP required to form the $\alpha$-CDP(ss) phase. That is, under the 1 °C/min heating rate used in the thermal analysis studies, the eutectoid reaction evidently does not reach completion until 180 °C. In contrast, equilibration at 160 °C in the diffraction experiment was apparently possible due to the slower effective heating rate, in which data were acquired after a 20 min hold at the measurement temperature. Rietveld analysis (Figure S5) showed this pattern, as in the $x$ = 2/9 case, to be consistent with the structure of cubic superprotonic CDP, with the exception of having a distinctly larger lattice constant. However, the cell volume of the $\alpha$-CDP(ss) obtained at $x$ = 0.18 was substantially smaller than that obtained from the $x$ = 2/9 material, a phenomenon discussed further below. The thermal expansion behavior of $\alpha$-CDP(ss) at the eutectoid composition, now captured over the temperature range of 160−178 °C, was again unremarkable (Figure 3c).
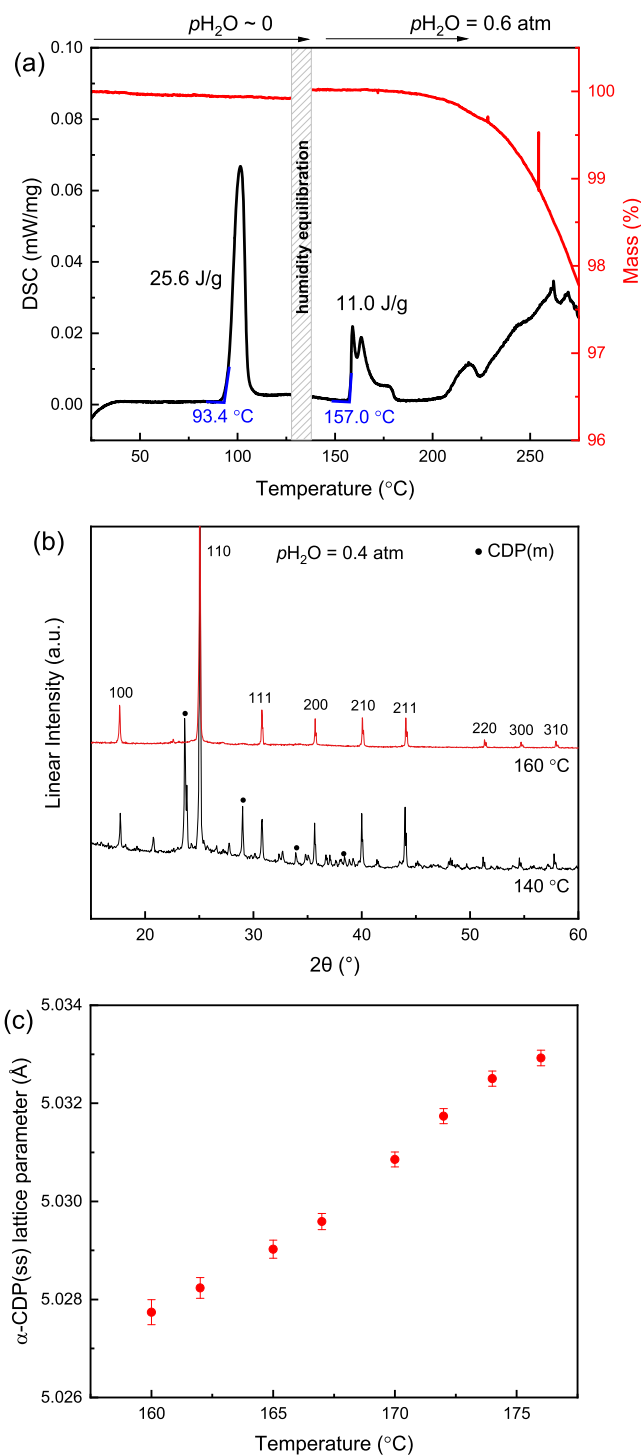


**Figure 3.** Phase transformation behavior of $(1-x)CsH_2PO_4 - xH_3PO_4$ at $x$ = 0.18, the eutectoid composition: (a) XRD patterns measured at the temperatures indicated with the inset showing cubic lattice parameter; (b) simultaneously measured TGA/DSC profiles at a heating rate of 1°C/min; and (c) lattice constant obtained from Rietveld refinement as a function of temperature. Data in (a) at temperatures of 130 °C and above were collected with the sample chamber atmosphere maintained at $pH_2O$ = 0.4 atm (balance $N_2$), whereas those in (b) were collected with sample chamber atmosphere maintained at $pH_2O$ = 0.6 atm (balance Ar). Data reflecting system equilibration to the high-humidity condition at 130 °C are omitted from (b). The results reveal the transitions CDP(m) + $CsH_5(PO_4)_2$ → CDP(m) + CPP @ 90 °C and CDP(m) + CPP → $\alpha$-CDP(ss) @ 160 °C.

The $^{31}$P and $^1$H NMR results for the $x = 0.18$ material, Figures 4 and 5, respectively, generally agree with the XRD and DSC findings. The spectra collected at 140 °C show the
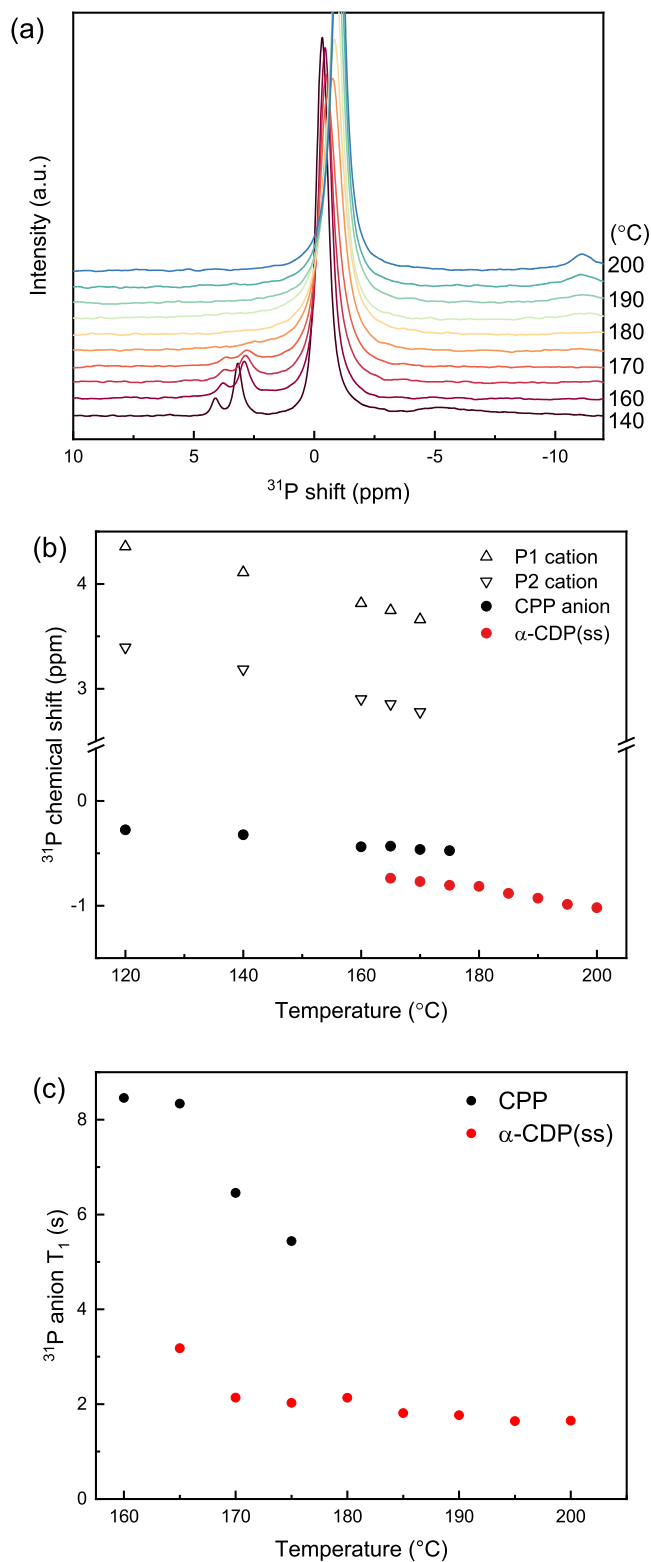
**Figure 4.** Variable-temperature $^{31}$P NMR measurements of $(1-x)$CsH$_2$PO$_4$ $- x$H$_3$PO$_4$ at $x = 0.18$, the eutectoid composition: (a) spectra collected at indicated temperatures; (b) chemical shifts as a function of temperature; and (c) $T_1$ relaxation time of the ∼0 ppm resonance as a function of temperature.
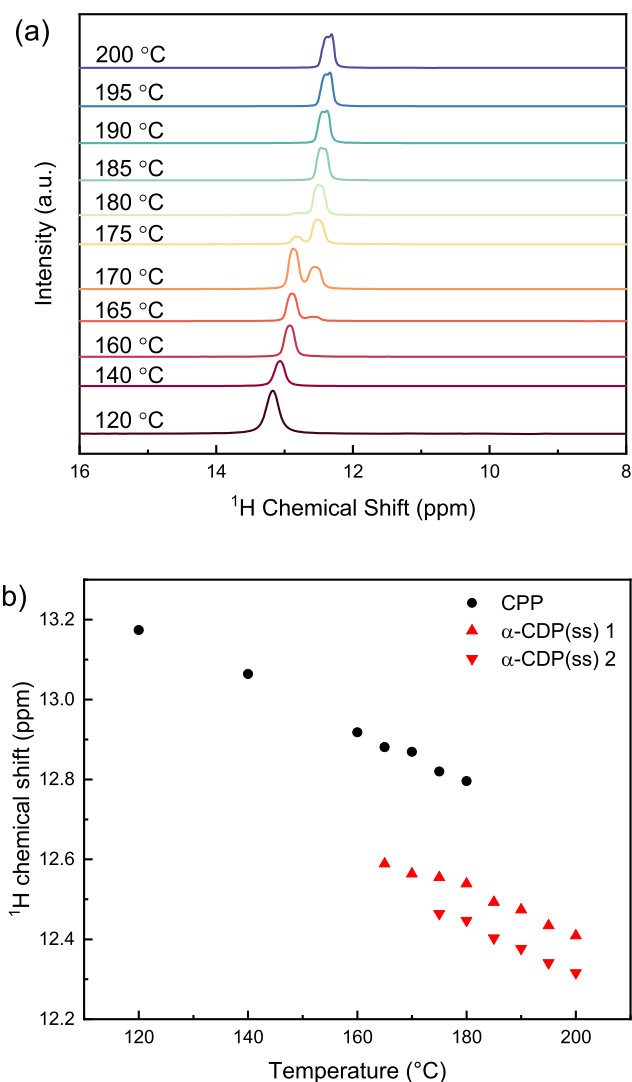
**Figure 5.** Variable-temperature $^1$H NMR measurements of $(1-x)$CsH$_2$PO$_4$ $- x$H$_3$PO$_4$ at $x = 0.18$, the eutectoid composition: (a) spectra collected at indicated temperatures and (b) chemical shifts as a function of temperature.

sample existed as a two-phase mixture of CDP(m) and CPP. CPP is represented in the $^{31}$P spectrum at this temperature by the two cation-site phosphorus resonances (4.6 and 3.7 ppm) as well as the anion-site phosphorus resonance (0.3 ppm),[12] whereas in the $^1$H spectra, it is represented by the sharp resonance at 13.2 ppm (at 120 °C). The presence of CDP(m) is more difficult to discern given its relatively low molar fraction of the sample (<20%) and the broader resonances characteristic of this phase. Nevertheless, its presence can be observed in the $^{31}$P spectra as a broad resonance at −4.5 ppm and in the $^1$H spectra as a broad feature at ∼11.6 ppm (Figure S6, too small for Figures 4a and 5a). These resonances are consistent with previous reports for CDP(m),[14,15] though it is noted that the expected proton resonance of CDP(m) at ∼14 ppm is obscured by the larger CPP resonance. Heating induces changes in the spectra that reflect the formation of single-phase α-CDP(ss). In the $^1$H spectra (Figure 5), a new resonance emerges at 165 °C at a shift of 12.6 ppm and grows with temperature at the expense of the CPP resonance now at 12.9 ppm, until the latter is no longer observed at 185 °C. The coexistence of signals from the two phases from 165 to 180 °C
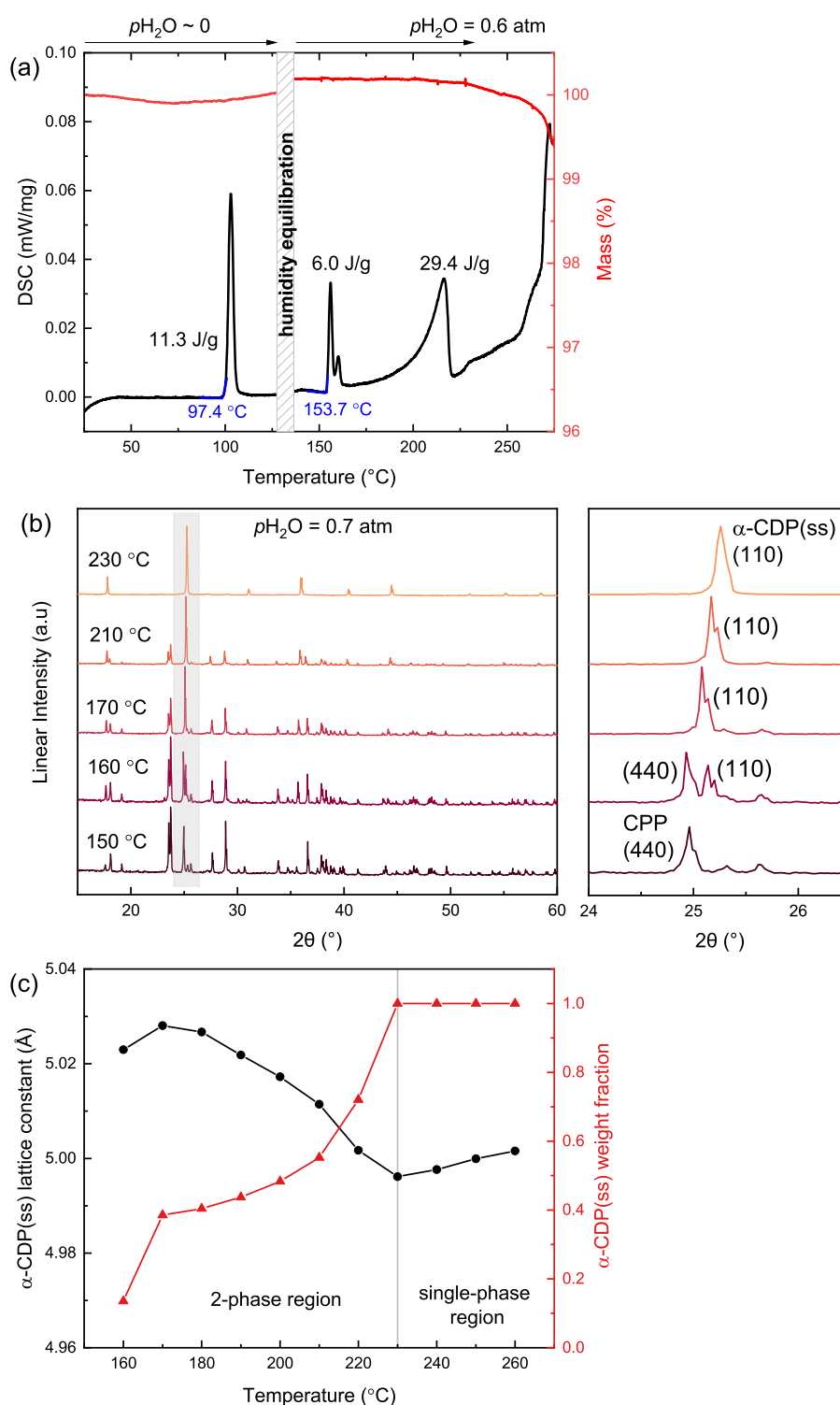
**Figure 6.** Phase transformation behavior of $(1-x)CsH_2PO_4 - xH_3PO_4$ at $x = 0.07$: (a) Simultaneously measured TGA/DSC profiles at a heating rate of 1 °C/min; (b) XRD patterns measured at the temperatures indicated; and (c) lattice constant and weight fraction as functions of temperature (uncertainties in the refined values fall within the span of the datapoint symbols). (a) $pH_2O = 0.6$ atm (balance Ar) was introduced at 130 °C as part of the heating protocol, and data reflecting system equilibration to the high-humidity condition are omitted. (b) Sample chamber atmosphere maintained at $pH_2O = 0.7$ atm (balance $N_2$). (c) Lines between points serve only to guide the eye and do not reflect sample behavior between measurement temperatures. The results reveal the transitions $CDP(m) + CsH_5(PO_4)_2 \rightarrow CDP(m) + CPP$ @ 90 °C and $CDP(m) + CPP \rightarrow CDP(m) + \alpha\text{-}CDP(ss)$ @ 160 °C.

is attributed to the sluggish kinetics of the reaction, as discussed in the context of the thermal behavior, along with a likely thermal gradient in the rotor, rather than thermodynamic equilibrium between the two compounds. A close examination

of the high-temperature spectra indicates a splitting of the new $^1H$ peak (Figure S7a), potentially due to $^{31}P\text{-}^1H$ J-coupling, but the effect was not further explored. In the $^{31}P$ spectra (Figure 4), the consumption of CPP is evident by the loss of intensity

from the cation-site resonances, an effect that initiates at 160 °C and appears complete by 175 °C. Simultaneously, the resonance associated with the anion-site phosphorous, at −0.4 ppm at 160 °C, broadens and is resolvable into two peaks over the temperature range of 165−175 °C (Figure S7b). The emergent, slightly upfield peak within this pair is attributed to $\alpha$-CDP(ss). Its position, after accounting for the obvious temperature dependence evident in Figure 4b, is similar to that of the phosphorus resonance in superprotonic stoichiometric CDP, which occurs at a shift of −1.8 ppm[22] at 250 °C. Distinct $T_1$ relaxation times were measured for the two anion-site resonances, Figure 4c, with faster dynamics indicated in $\alpha$-CDP(ss) ($T_1 \approx 2$ s) than CPP ($T_1$ decreasing with temperature from ≈8 s to ≈5 s). At 180 °C and above, only the anion-site phosphorus resonance remains, indicating that this is the sole phosphorus environment in $\alpha$-CDP(ss).

Turning to the behavior in the Cs-rich region of the phase diagram ($x = 0.07$), Figure 6, the two-phase mixture of CDP(m) and $CsH_5(PO_4)_2$ present at ambient temperature reacted on heating to form CPP and excess CDP(m). Similar to the other compositions, the endothermic formation of CPP occurred, without mass loss, Figure 6a, but in this case, the reaction kinetics were slightly retarded, and the thermal signal was detected with an onset at 97 °C. The diffraction pattern collected at 150 °C revealed stoichiometric quantities of the two phases (CPP and CDP(m)), Figure 6b. On further heating, the mixture underwent a second reaction at 154 °C to yield eutectoid $\alpha$-CDP(ss), now in equilibrium with excess CDP(m). The thermal signature reveals a binodal peak that initiates at this temperature, similar to that observed for the eutectic composition (Figure 3a). The formation of $\alpha$-CDP(ss) can be clearly seen in the diffraction pattern collected at 160 °C from the presence of the (110) peak of this phase at $2\theta = 25.1°$ (Figure 6b, see also Figure S8). The lattice parameter of $\alpha$-CDP(ss) at 160 °C was 5.028(5) Å, essentially identical to that found for the sample with the eutectoid composition (5.0277(3) Å). The diffraction data further revealed the presence of residual CPP at 160 °C, even though, in principle, this phase is not expected to coexist with $\alpha$-CDP(ss) under such conditions ($T = 160$ °C, $x = 0.07$); this is likely due to a small thermal gradient across the sample stage. Increasing the temperature to 170 °C induced the reaction of the remaining CPP, leaving a two-phase mixture of $\alpha$-CDP(ss) and CDP(m). Further heating between 170 and 230 °C resulted in a gradual consumption of CDP(m) by dissolution into the $\alpha$-CDP(ss) phase as evidenced in the diffraction data by a decrease in the CDP(m) peak intensities and an increase in the intensities of the peaks due to $\alpha$-CDP(ss). The dissolution was detected in the thermal data by a long and substantial endothermic event, which peaked at 216.5 °C. This process was moreover accompanied by a *decrease* in the cell parameter of $\alpha$-CDP(ss) (Figure 6c), which terminated only with the complete consumption of CDP(m) at 230 °C. Positive linear thermal expansion of $\alpha$-CDP(ss) was observed at temperatures above 230 °C. Thus, the lattice contraction of $\alpha$-CDP(ss) with heating is concluded to be a result of CDP(m) incorporation and the accompanying change in composition. In contrast, CDP(m) underwent conventional thermal expansion, consistent with previous characterizations of this phase[23] (Figure S9a).

It is to be emphasized that all of the phase transitions discussed above occurred in the absence of mass loss, as shown unequivocally by the differential thermal gravimetric (dTG) profiles derived from TGA profiles reported in Figures 2a, 3a, and 6a. The dTG analysis reveals a decreasing stability limit with increasing $x$. Specifically, with a 0.6 atm partial pressure of steam, CDP ($x = 0$) is known to dehydrate at $T_d = 284$ °C.[24] Here, mass loss was observed to initiate under $pH_2O = 0.6$ atm at $T_d = 225$ °C, 184 °C, and 180 °C, respectively, when $x = 0.07$, 0.18, and 2/9, respectively. At the composition of CPP, the $\alpha$-CDP(ss) phase is thus barely captured under $pH_2O = 0.6$ atm before decomposition occurs. A widening of the stability window under higher $pH_2O$ (as expected thermodynamically) has been shown elsewhere.[21] Here, the decomposition of the other compositions has not been studied systematically and the quoted temperatures for the onset of mass loss reflect the lower bounds for material stability.

The decrease in unit cell constant beyond the eutectoid temperature for the $\alpha$-CDP(ss) phase observed in the $x = 0.07$ sample (Figure 6c) was attributed in the discussion above to changes in composition arising from the dissolution of stoichiometric CDP(m), $CsH_2PO_4$, into the nonstoichiometric $\alpha$-$[Cs_{1−x}H_x]H_2PO_4(ss)$ phase. Examining the temperature dependence of the lattice parameters for all compositions studied (Figure 7, $x = 0$, 0.02, 0.05, 0.07, 0.15, 0.18, 2/9), it is evident that chemically induced contraction on heating is largely obeyed for all samples that exist as a two-phase mixture of $\alpha$-CDP(ss) and CDP(m). Upon the complete consumption of CDP(m), $\alpha$-CDP(ss), now isolated as a single phase, displays in all cases conventional linear thermal expansion. (Figure S10 shows the coincidence of the single-phase regions with the positive thermal expansion behavior.) The single-phase data moreover reveal a strong compositional dependence of the cell volume, with larger $x$ values resulting in larger lattice constants. After accounting for the influence of thermal expansion by extrapolating the measured lattice parameters to a common temperature of 170 °C, it is further evident that the lattice parameter depends linearly on composition $x$ in $\alpha$-$[Cs_{1−x}H_x]H_2PO_4(ss)$ (Figure 7b), in accordance with Vegard's law and with a slope of 0.46(3) Å/$x$. The smooth linear behavior indicates that the manner by which excess $H_3PO_4$ is incorporated into this phase is the same across the entire composition range examined. This expansion with $x$ is entirely consistent with the observed contraction on heating in the two-phase region. Furthermore, the consistency of the chemical contraction in the two-phase region across samples indicates a shared composition trend, or solvus line, that exists between the eutectoid point and the superprotonic transition of CDP. At lower temperatures, 160−170 °C, $\alpha$-CDP(ss) undergoes expansion rather than contraction (Figure 7a), despite existing in equilibrium with CDP(m). This implies that the composition change just above the eutectoid temperature must be small, allowing thermal expansion effects to dominate the behavior, which in turn implies that the solvus line must be relatively steep from 155 to 170 °C.

In contrast to $\alpha$-CDP(ss), the cell volumes of the CDP(m) and CPP phases did not significantly deviate from those of the stoichiometric phases at any of the temperatures at which these phases were observed (Figure S9). Thus, CDP(m) and CPP exhibit little to no nonstoichiometry in the phase space characterized here, and they are accurately represented as line compounds on the phase diagram. Observed in this study was also an unusual reversible mass loss in $\alpha$-CDP(ss) phase in response to changes in temperature and steam partial pressure, which was accompanied by a slight change in cell volume (Figure S11). In the two-phase region, however, there was no
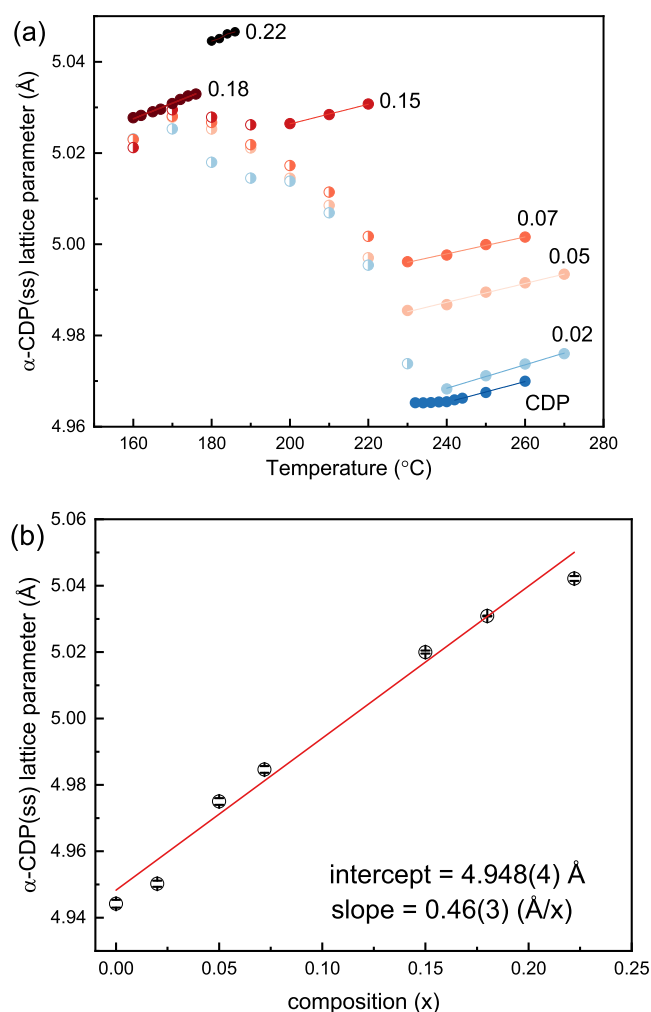
**Figure 7.** Lattice parameters of the $\alpha$-CDP(ss) phase of various sample compositions, $x$: (a) thermal evolution of the lattice parameter, with $x$ as indicated, at $p\mathrm{H_2O}$ between 0.4 and 0.7 atm, as required for suppressing dehydration and (b) lattice parameters of single-phase $\alpha$-CDP(ss) as a function of composition, upon extrapolation to 170 °C. In (a), filled symbols indicate the presence of only $\alpha$-CDP(ss) in the diffraction pattern, whereas half-filled symbols indicate the coexistence with CDP(m). The linear trend of lattice parameter with composition is consistent with the empirical Vegard's law. In (a), uncertainties in the refined values fall within the span of the datapoint symbols (Figure S10), as they do in (b), and are omitted here for visual clarity.

impact on cell volume, implying no impact on the chemically induced thermal contraction (Figure S11c).

**3.3. Solvus Line Determination.** Most commonly, the determination of the solvus line (where the term is used here to refer to the boundary between the two-phase $\alpha$-CDP(ss) + CDP(m) region and the single-phase $\alpha$-CDP(ss) region) in a phase diagram such as that in Figure 1 is achieved by quantifying the molar fractions of components in equilibrated mixtures within the two-phase region or establishing the temperature at which the low-temperature phase is no longer detected. The requisite data are typically obtained by diffraction studies. The former approach requires reliable detection of the minority phase in the diffraction data, ideally at multiple global compositions, whereas the latter requires measurements in small temperature steps to accurately reveal the boundary, particularly if the boundary is shallow. Applying

these standard approaches to the data collected here at five compositions within the two-phase region using 10 °C temperature steps produced reasonable datapoints for the solvus boundary, but with a large scatter (Figure S11). The uncertainty in the solvus position was particularly high at a low $x$, where, for example, phase analysis suggested possible retention of CDP(m) in the $x = 0.02$ sample at a temperature as high as 230 °C. In light of the transition temperature in stoichiometric CDP of 228 °C,[24] such behavior is thermodynamically forbidden in a eutectoid system.

An alternative and more accurate approach is pursued here by recognizing that at each diffraction measurement in the two-phase region, the composition and hence lattice parameter of $\alpha$-CDP(ss) depends only on temperature and is independent of the global composition. Thus, embedded in the lattice parameter data in Figure 7 is the composition of the phase boundary at each measurement temperature. If one considers a temperature of 210 °C, for example, each of the measurements of samples with global compositions $x = 0.07$, 0.05, and 0.02, reflects the lattice parameter of $\alpha$-CDP(ss) at the phase boundary at 210 °C. In principle, the three datapoints, with an average lattice parameter value of 5.009 Å, should fully overlap, but they are slightly distinct due to experimental uncertainties. In the case of the $x = 0.02$ composition, the quantity of $\alpha$-CDP(ss) in the two-phase mixtures is small, particularly at temperatures just above the eutectoid temperature, and hence the uncertainty in the cell parameter for measurements in this region is high. Nevertheless, accuracy is gained from this approach because the determination of the lattice parameter of a cubic material is generally more reliable than the determination of phase fractions. In this system in particular, peak intensities in the high-temperature diffraction patterns were found to be impacted by grain coarsening induced by the solid-state reactions; the transformation to a smaller number of large-sized crystallites removed the randomness generally required for interpreting peak intensities in terms of phase fractions. From an average of the reliable cell parameters of $\alpha$-CDP(ss) in the two-phase measurements, we generate the lattice parameter of the composition at the phase boundary ($a_b$) as a function of temperature (Figure 8). In turn, the lattice parameter of the $\alpha$ phase, $a_\alpha$, can be treated, to a first



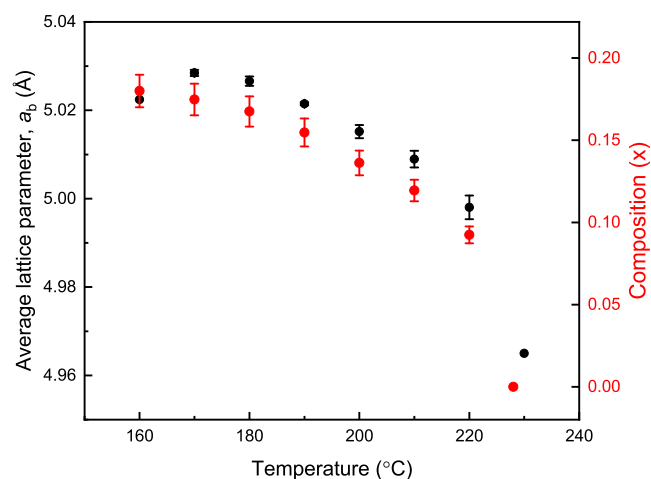**Figure 8.** Determination of the solvus boundary: temperature dependence of the cell parameter of $\alpha$-CDP(ss) at the boundary between the $\alpha$-CDP(ss)+CDP(m) and $\alpha$-CDP(ss) regions and inferred composition of $\alpha$-CDP(ss) at the boundary.

approximation, as the sum of the thermal expansion and the chemical expansion terms

$$a_a(x_c, T) = a_{a,0} + B*x_c + D*T; \quad a_{a,0} = 4.948(4)$$

$$\text{Å}, \ B = 0.46(3) \ \text{Å}/x_c, \ \text{and} \ D = 2.2(1) \times 10^{-4} \ \text{Å}/°C$$

where $x_c$ is the composition of $\alpha$-CDP(ss), $\Delta T = T$-170 °C, and $T$ is the temperature (in °C). The term $D$ is determined by averaging over the thermal expansion behavior of all compositions of $x \leq 0.15$ (Figure S9). Inverting the above with $a_\alpha$ set to $a_b$, we solve for the composition at the phase boundary at each temperature between 160 and 220 °C. This phase-boundary composition result is shown in Figure 8, alongside the lattice parameter result, as well as in Figure 1. The scatter is much smaller than in the case of the direct determination of the phase boundary (Figure S11).

**3.4. Structure and Chemistry of $\alpha$-CDP(ss).** The crystal structure of stoichiometric, superprotonic CDP is well known. In this state, the material adopts the CsCl structure-type with the $H_2PO_4$ anion residing on the Cl site and displaying nearly free rotational disorder. The observation in the present study of a material with stoichiometry $[Cs_{1-x}H_x]H_2PO_4$ in the same phase space as cubic $CsH_2PO_4$ implies that the superprotonic structure can accommodate unusual types of point defects. In particular, the $Cs/PO_4$ ratio of less than 1 requires either (i) the presence of Cs vacancies (charge-balanced by proton interstitials, which would presumably form neutral $H_3PO_4$ groups); (ii) the presence of $H_3PO_4$ interstitials, a highly unlikely scenario given the density of packing in the CsCl structure-type; or (iii) similar to CPP, the occurrence of antisite defects in which $H_4PO_4^+$ cations replace Cs species. The experimental data strongly point toward the first of these scenarios, the occurrence of Cs vacancies. The proposed structure is shown schematically in Figure 9, where the partial
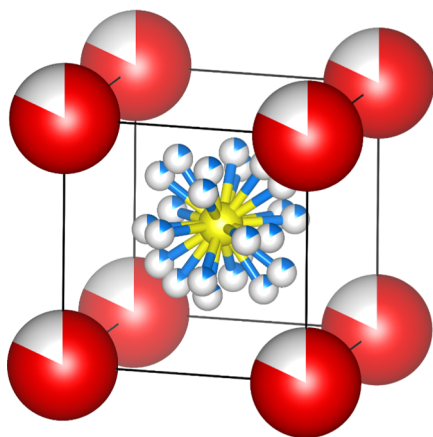


**Figure 9.** Schematic of the $\alpha$-CDP(ss) structure. The multiple orientations of the phosphate anion represent the rotational disorder characteristic to superprotonic phases. The Cs site is partially occupied with a random distribution of vacancies. Protons are omitted from the figure.

occupancy of the Cs site denotes the disordered vacancies. A key indicator of Cs vacancy formation is the significant contraction of the subcell volume at the CPP to $\alpha$-CDP(ss) transition (Figure 2). Prior to the transition, the subcell volume of CPP is substantially larger than that of stoichiometric, superprotonic CDP. This expansion occurs because the $H_4PO_4^+$ ions are larger than the $Cs^+$ cations which

they replace. A CPP $\rightarrow \alpha$-CDP(ss) transition involving only a disordering of the $Cs^+$ and $H_4PO_4^+$ cations, and hence the creation of antisite defects in the latter, would be expected to have very little impact on the subcell volume. In contrast, elimination of the large polycations from the cation sites would very plausibly decrease the subcell volume, as observed. Attempts to confirm the presence of Cs vacancies by Rietveld refinement of the Cs site occupancy were, however, unsuccessful. This is attributed to the inherent challenge of high correlation between displacement parameter and occupancy factor in any structure analysis and the specific challenge here of the coarsening of the microstructure through the high-temperature reactions that form CPP and especially $\alpha$-CDP(ss).

Further evidence of the absence of antisite defects ($H_4PO_4^+$ species residing on the cation sites in $\alpha$-CDP(ss)) is provided by the NMR data discussed above. The $^{31}P$ NMR spectra (Figure 4) revealed that the disordered anion phosphate is the only phosphorus resonance associated with the $\alpha$-CDP(ss) phase. In the $^1H$ NMR spectra (Figure 5), the very slight splitting of the high-temperature resonance appears too small to be a consequence of antisite defects. The overall position of the peak suggests that the excess protons in $\alpha$-CDP(ss) are largely indistinguishable in both position and motion from the protons in conventional cubic CDP.

Accepting that Cs deficiency in $\alpha$-$[Cs_{1-x}H_x]H_2PO_4$ is accommodated by the presence of Cs vacancies, it is at first glance surprising that the lattice constant increases with $x$. The result suggests that in the absence of a Cs cation, unmitigated electrostatic repulsion of the eight nearest-neighbor phosphate groups causes expansion, despite the likelihood that, for reasons of overall charge balance, some of the phosphate groups are neutral $H_3PO_4$ species. In the case of Rb- and K-substituted CDP ($[Cs_{1-x}Rb_x]H_2PO_4$ and $[Cs_{1-x}K_x]H_2PO_4$), contraction occurs,[16] consistent with the presence of a smaller isovalent species on the Cs site.

**3.5. Conductivity.** The conductivity of the materials studied here (in the heating cycle) is summarized in Figure 10. The behavior of CDP fully agrees with prior reports,[4] with a sharp, 3 orders of magnitude increase in conductivity at the monoclinic-to-cubic transition that initiates at 228 °C. For the samples with $x = 2/9$ (equivalent to CPP) and 0.18, the formation of CPP is evident from the moderate jump in conductivity that initiates at ≈100 °C, reasonably close to the CPP formation temperature of ≈90 °C detected by thermal analysis. At 125 °C, at which all compositions (except the end-members) exist as a two-phase mixture of CDP(m) and CPP, the conductivity generally increases with $x$. This reflects the higher conductivity of CPP than CDP(m) and the simple two-phase mixing behavior. For all two-phase samples except $x = 0.02$, a further moderate jump in conductivity that initiates at ≈150 °C is evident, reflecting the formation of $\alpha$-CDP(ss). At the eutectoid composition ($x = 0.18$), the transition produces single-phase $\alpha$-CDP(ss), which has a slightly higher conductivity than that of single-phase CPP ($2.61(8) \times 10^{-3}$ vs $1.19(3) \times 10^{-3}$ S cm$^{-1}$ @ 158 °C), consistent with the slightly shorter $T_1$ relaxation time for the phosphorus in the anion group phosphate in CDP than in CPP, Figure 4a. The slightly lower conductivity of CPP than CDP, despite the crystallographic similarities of the two structures, was noted in our previous study.[21] Here, because of ready dehydration of the $x = 2/9$ composition at a high temperature, the impact of the 180 °C phase transformation of CPP to $\alpha$-CDP(ss) could not
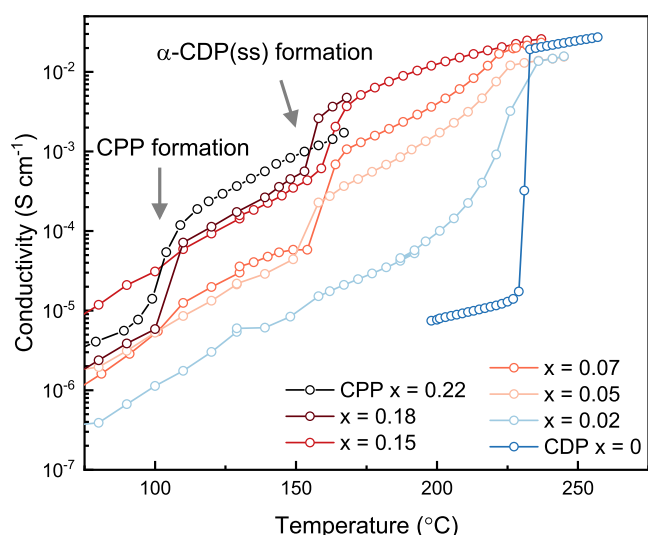
**Figure 10.** Conductivity of materials in the $(1-x)CsH_2PO_4 - xH_3PO_4$ system as a function of temperature on heating with compositions as indicated (conductivity of $x = 0.22$ composition from ref 21 with permission from the American Chemical Society). Data above 130 °C are collected under high $pH_2O$: 0.69 atm for $x = 0.18$, 0.15, and 0.07, and 0.47 atm for $x = 0.05$ and 0.02. The phase transition corresponding to the formation of CPP from CDP(m) and $CsH_5(PO_4)_2$ at ≈90 °C is evident in the behavior of the compositions with large $x$ (0.22 and 0.18), and the formation of $\alpha$-CDP(ss) at ≈150 °C, approximately the eutectic temperature, is evident in compositions with a moderate to large $x$ (0.05, 0.07, 0.15, and 0.18). In the single-phase region, the conductivity is largely insensitive to composition.

be observed. Within the two-phase region of CDP(m) and $\alpha$-CDP(ss) (observed in samples with $x < 0.18$ above 155 °C), the conductivity generally increases with $x$, again reflecting the fact that the superprotonic $\alpha$-CDP(ss) phase accounts for a greater proportion of the material. In contrast to the behavior below the eutectoid temperature, however, the low $x$ compositions show upward concavity in the $\sigma(T)$ profiles, a feature taken to reflect the increasing $\alpha$-CDP(ss) content with temperature. The nonmonotonic trend with composition at a low temperature, below the CPP formation, likely reflects differing levels of $H_2O$ adsorption by the highly deliquescent $CsH_5(PO_4)_2$ compound.

The conductivities measured upon cooling through the solvus boundary were largely consistent with those obtained on heating, and only slight hysteresis was detected at the eutectoid temperature for those samples investigated in this regard (Figure S12). Notably, however, elevated conductivity was generally retained at temperatures below that corresponding to CPP decomposition into CDP(m) and $CsH_5(PO_4)_2$. This reflects the tendency of CPP to be retained as a metastable state outside of its stability limits, to as low as 80 °C.[21]

An important feature of the conductivity of $\alpha$-CDP(ss) is its weak sensitivity to composition $x$ (in its stoichiometry $[Cs_{1-x}H_x]H_2PO_4$) both in terms of absolute conductivity and activation energy in the single-phase region. While a small systematic trend may have been obscured as a result of experimental uncertainty, the absence of a detectable impact is somewhat surprising given the significant influence of composition on both proton concentration and unit cell dimensions (Figure 7b). It is of some value to compare this behavior to that of Rb- and K-substituted CDP. Both these

dopants reduced conductivity and induced lattice contraction, but the detrimental impact of K on proton transport at equivalent lattice contraction was far more pronounced than that of Rb.[16] Thus, the impact of cation chemistry on proton transport extends beyond structural influences—a conclusion again found in the present study where no clear correlation between lattice expansion and conductivity is observed. In the $CsHSO_4-CsH_2PO_4$ system, which forms a solid solution in the cubic superprotonic phase at a high temperature, the conductivity decreases with increasing $CsH_2PO_4$ and correspondingly proton content.[25] This result implies that the proton concentration similarly plays a secondary role in establishing the conductivity.

Regardless of the subtlety of the role of material stoichiometry, the overall high conductivity of $\alpha$-CDP(ss) indicates that the proton transport mechanism is analogous to that in stoichiometric CDP, *i.e.*, it involves rapid phosphate group reorientation and proton transfer between neighboring polyanionic groups. Rapid anion reorientation is indeed evident from the sharpness of the $^{31}P$ NMR peak at −1.2 ppm, Figure 4a. The high conductivity of $\alpha$-[$Cs_{1-x}H_x]H_2PO_4$ at temperatures well below the superprotonic transition of stoichiometric $CsH_2PO_4$ has potential implications for electrochemical devices. In particular, a decrease in operating temperature may decrease the energy costs of generating high levels of $pH_2O$ at a high temperature as required to stabilize $CsH_2PO_4$ against decomposition by dehydration.[24] The material of composition $x = 0.15$, with conductivity exceeding $5 \times 10^{-3}$ S cm$^{-1}$ over the temperature range of 160−235 °C, appears especially attractive in this regard.

## 4. SUMMARY AND CONCLUSIONS

This work reveals that cubic CDP accommodates chemical off-stoichiometry with a formula described as $[Cs_{1-x}H_x]H_2PO_4$ for $x$ at least as large as 2/9. Excess $H_3PO_4$ units are incorporated into the cubic structure via the creation of vacancies on the cation sites that are charge-balanced by the excess protons. The $(1-x)CsH_2PO_4 - xH_3PO_4$ phase diagram in the $0 \leq x \leq 2/9$ range obeys eutectoid behavior, anchored, at temperatures above 90 °C, by stoichiometric, monoclinic CDP at $x = 0$ and stoichiometric $Cs_7(H_4PO_4)(H_2PO_4)_8$ at $x = 2/9$. The eutectoid reaction at which $\alpha$-CDP(ss) forms from these two precursors occurs at 155 °C and $x = 0.18$. A surprising feature of $\alpha$-CDP(ss) is the increase in cell volume with increasing chemical replacement of $Cs^+$ by $H^+$. The behavior is proposed to reflect the formation of cation site vacancies, with protons becoming associated with phosphate groups, as opposed to the occupation of cation sites by protons. The expansive effect of Cs deficiency in $\alpha$-CDP(ss) manifests as a chemically induced unit cell contraction when the phase is heated under equilibrium conditions alongside monoclinic CDP; heating in this two-phase region induces gradual dissolution of the stoichiometric monoclinic phase into $\alpha$-CDP(ss), thereby reducing the Cs deficiency in the latter. This behavior was exploited to establish the position of the solvus line boundary between $\alpha$-CDP(ss) and the two-phase region composed of monoclinic CDP and $\alpha$-CDP(ss). The concept of cation off-stoichiometry, in which protons replace large cations chemically but not structurally, presents a new approach in the design of superprotonic solid acid electrolytes and specifically the formation of superprotonic phases.

The conductivity of $\alpha$-CDP(ss) is surprisingly insensitive to the compositional off-stoichiometry. Furthermore, the eutec-

toid reaction temperature of $\alpha$-CDP(ss), 155 °C, is substantially lower than the superprotonic transition temperature of stoichiometric CDP, 228 °C, and the solvus boundary between $\alpha$-CDP(ss) and the two-phase, monoclinic CDP and $\alpha$-CDP(ss) region is relatively steep near the eutectoid composition. Combined, these effects result in high conductivity in compositions slightly rich in CDP relative to the eutectoid composition at temperatures well below the superprotonic transition of stoichiometric CDP. The excellent proton conductivities exhibited by these $\alpha$-CDP(ss) phases present an opportunity to extend the low-temperature operating limit of devices based on superprotonic solid acid electrolytes.

## ■ ASSOCIATED CONTENT

### Ⓢ Supporting Information

The Supporting Information is available free of charge at https://pubs.acs.org/doi/10.1021/acs.chemmater.1c04061.

> Rietveld refinement results; differential gravimetric analysis; zoomed NMR spectra; lattice parameter and phase fraction evolution with temperature; thermal expansion behavior; influence of humidity on mass and lattice parameter; alternative derivation of phase diagram; and conductivity on cooling (PDF)

## ■ AUTHOR INFORMATION

### Corresponding Author

Sossina M. Haile − Materials Science and Engineering, Northwestern University, Evanston, Illinois 60208, United States; Applied Physics, Northwestern University, Evanston, Illinois 60208, United States; ⓞ orcid.org/0000-0002-5293-6252; Email: sossina.haile@northwestern.edu

### Authors

Louis S. Wang − Materials Science and Engineering, Northwestern University, Evanston, Illinois 60208, United States; ⓞ orcid.org/0000-0003-4046-2341

Sawankumar V. Patel − Department of Chemistry and Biochemistry, Florida State University, Tallahassee, Florida 32306, United States; ⓞ orcid.org/0000-0002-5293-9330

Erica Truong − Department of Chemistry and Biochemistry, Florida State University, Tallahassee, Florida 32306, United States

Yan-Yan Hu − Department of Chemistry and Biochemistry, Florida State University, Tallahassee, Florida 32306, United States; Center of Interdisciplinary Magnetic Resonance, National High Magnetic Field Laboratory, Tallahassee, Florida 32310, United States; ⓞ orcid.org/0000-0003-0677-5897

Complete contact information is available at:
https://pubs.acs.org/10.1021/acs.chemmater.1c04061

### Notes

The authors declare no competing financial interest.

## ■ ACKNOWLEDGMENTS

## ■ REFERENCES

(1) Merinov, B. V. Mechanism of proton transport in compounds having a dynamically disordered hydrogen bond network. Solid State Ionics 1996, 84, 89−96.

(2) Baranov, A. Crystals with disordered hydrogen-bond networks and superprotonic conductivity. Review. Crystallogr. Rep. 2003, 48, 1012−1037.

(3) Haile, S. M.; Boysen, D. A.; Chisholm, C. R. I.; Merle, R. B. Solid acids as fuel cell electrolytes. Nature 2001, 410, 910−913.

(4) Haile, S. M.; Chisholm, C. R. I.; Sasaki, K.; Boysen, D. A.; Uda, T. Solid acid proton conductors: from laboratory curiosities to fuel cell electrolytes. Faraday Discuss. 2007, 134, 17−39.

(5) Boysen, D. A.; Cha, S.; Chisholm, C. R. I.; Giapis, K. P.; Haile, S. M.; Papandrew, A. B.; Sasaki, K. A. From Laboratory Breakthrough to Technological Realization: The Development Path for Solid Acid Fuel Cells. Electrochem. Soc. Interface 2009, 18, 53−59.

(6) Boysen, D. A.; Uda, T.; Chisholm, C. R. I.; Haile, S. M. High-performance solid acid fuel cells through humidity stabilization. Science 2004, 303, 68−70.

(7) Merle, R. B.; Chisholm, C. R. I.; Boysen, D. A.; Haile, S. M. Instability of sulfate and selenate solid acids in fuel cell environments. Energy Fuels 2003, 17, 210−215.

(8) Baranov, A. I.; Khiznichenko, V. P.; Sandler, V. A.; Shuvalov, L. A. Frequency Dielectric-Dispersion in the Ferroelectric and Superionic Phases of $CsH_2PO_4$. Ferroelectrics 1988, 81, 183−186.

(9) Bronowska, W.; Pietraszko, A. X-ray Study of the High-Temperature Phase-Transition of $CsH_2PO_4$ Crystals. Solid State Commun. 1990, 76, 293−298.

(10) Bagryantseva, I. N.; Gaydamaka, A. A.; Ponomareva, V. G. Intermediate temperature proton electrolytes based on cesium dihydrogen phosphate and Butvar polymer. Ionics 2020, 26, 1813−1818.

(11) Lavrova, G. V.; Shutova, E. S.; Ponomareva, V. G.; Dunyushkina, L. A. Proton conductivity and interphase interaction in $CsH_2PO_4$-$SrZrO_3$ composites. Russ. J. Electrochem. 2013, 49, 718−724.

(12) Leal, J. H.; Martinez, H.; Martinez, I.; Price, A. D.; Goos, A. G.; Botez, C. E. Stability of the superprotonic conduction of (1-x)$CsH_2PO_4$/$xSiO_2$ ($0 \leq x \leq 0.3$) composites under dry and humid environments. Mater. Today Commun. 2018, 15, 11−17.

(13) Otomo, J.; Ishigooka, T.; Kitano, T.; Takahashi, H.; Nagamoto, H. Phase transition and proton transport characteristics in $CsH_2PO_4$/$SiO_2$ composites. Electrochim. Acta 2008, 53, 8186−8195.

(14) Ponomareva, V. G.; Bagryantseva, I. N.; Shutova, E. S. Hybrid systems based on nanodiamond and cesium dihydrogen phosphate. Mater. Today Proceedings 2020, 25, 521−524.

(15) Boysen, D. A.; Chisholm, C. R. I.; Haile, S. M.; Narayanan, S. R. Polymer solid acid composite membranes for fuel-cell applications. J. Electrochem. Soc. 2000, 147, 3610−3613.

(16) Ikeda, A.; Kitchaev, D. A.; Haile, S. M. Phase behavior and superprotonic conductivity in the $Cs_{1-x}Rb_xH_2PO_4$ and $Cs_{1-x}K_xH_2PO_4$ systems. J. Mater. Chem. A 2014, 2, 204−214.

(17) Ponomareva, V. G.; Bagryantseva, I. N.; Shutova, E. S. Effect of Cation Substitution in $Cs_{1-2x}Ba_xH_2PO_4$ on Structural Properties and Proton Conductivity. Phys. Solid State 2017, 59, 1387−1394.

(18) Ponomareva, V. G.; Bagryantseva, I. N. The influence of $Cs_2HPO_4$ * $H_2O$ impurity on the proton conductivity and thermal properties of $CsH_2PO_4$. Solid State Ionics 2019, 329, 90−94.

(19) Singh, D.; Kumar, P.; Singh, J.; Veer, D.; Kumar, A.; Katiyar, R. S. Structural, thermal and electrical properties of composites electrolytes (1-x)$CsH_2PO_4$/$xZrO_2$ ($0 \leq x \leq 0.4$) for fuel cell with advanced electrode. SN Appl. Sci. 2021, 3, 7.

(20) Ponomareva, V. G.; Lavrova, G. V. Effect of the excess protons on the electrotansport, structural and thermodynamic properties of $CsH_2PO_4$. Solid State Ionics 2017, 304, 90−95.

(21) Wang, L. S.; Patel, S. V.; Sanghvi, S. S.; Hu, Y. Y.; Haile, S. M. Structure and Properties of $Cs_7(H_4PO_4)(H_2PO_4)_8$: A New Super-protonic Solid Acid Featuring the Unusual Polycation $(H_4PO_4)^+$. *J. Am. Chem. Soc.* **2020**, *142*, 19992−20001.

(22) Kim, G.; Blanc, F.; Hu, Y. Y.; Grey, C. P. Understanding the Conduction Mechanism of the Protonic Conductor $CsH_2PO_4$ by Solid-State NMR Spectroscopy. *J. Phys. Chem. C* **2013**, *117*, 6504−6515.

(23) Louie, M. W.; Kislitsyn, M.; Bhattacharya, K.; Haile, S. M. Phase transformation and hysteresis behavior in $Cs_{1-x}Rb_xH_2PO_4$. *Solid State Ionics* **2010**, *181*, 173−179.

(24) Ikeda, A.; Haile, S. M. The thermodynamics and kinetics of the dehydration of $CsH_2PO_4$ studied in the presence of $SiO_2$. *Solid State Ionics* **2012**, *213*, 63−71.

(25) Yamane, Y.; Yamada, K.; Inoue, K. Superprotonic solid solutions between $CsHSO_4$ and $CsH_2PO_4$. *Solid State Ionics* **2008**, *179*, 483−488.